Journal of Sound and Vibration (2001) **241**(3), 401–421
doi:10.1006/jsvi.2000.3289, available online at http://www.idealibrary.com on IDEAL®

ACOUSTIC BEHAVIOUR OF ELLIPTICAL CHAMBER MUFFLERS

F. D. Denia, J. Albelda and F. J. Fuenmayor

Departamento de Ingeniería Mecánica y de Materiales, Universidad Politécnica de Valencia, Camino de Vera s/n, E-46022 Valencia, Spain. E-mail: ffuenmay@mcm.upv.es

AND

A. J. Torregrosa

CMT. Departamento de Máquinas y Motores Térmicos, Universidad Politécnica de Valencia, Camino de Vera s/n, 46022 Valencia, Spain

(*Received* 27 *July* 1999, *and in final form* 3 *August* 2000)

The present work studies in detail the acoustic behaviour of mufflers with elliptical cross-section. The effect of the chamber length and the location of the inlet and outlet ports is considered. In addition, the eccentricity of the ellipse is taken into account, since it generates important discrepancies with respect to those results obtained for the case of circular chambers, mainly when practical values of eccentricity are considered. The analytical description of the acoustic behaviour of chambers with elliptical cross-section has been obtained via the truncated modal superposition method. First, the problem of natural frequencies and mode shapes has been approached by considering the Helmholtz equation in an elliptical domain, the solution of which can be expressed by means of Mathieu functions. Then, the frequency response functions of the muffler have been evaluated through truncated modal superposition. The results obtained are shown to compare well with those obtained from finite element calculations and experimental measurements. In addition, simple polynomial expressions have been developed in order to evaluate the cut-off frequency of concentric and non-concentric elliptical chambers, which is an important feature since higher order modes start to propagate without attenuation above this frequency. A simple polynomial expression is also developed to find the optimum location of the outlet port in order to extend the range of acoustic attenuation of the muffler. The influence of the geometry on the acoustic performance and the propagation of elliptic modes is studied for two configurations of interest, such as the expansion chamber and the reversing chamber muffler.

© 2001 Academic Press

1. INTRODUCTION

This work is justified basically by the wide use of elliptical geometry in automotive mufflers, in addition to the relatively few reported studies of its acoustic attenuation performance. Most of the references deal with rectangular and circular geometries, with their associated simplifications in the mathematical aspects when an analytical approach is considered.

The use of sudden area changes between pipes of different cross-section is one of the most important features in exhaust silencers. In the neighbourhood of sudden area changes, wave propagation is three-dimensional even in the low-frequency range, due to the generation of

0022-460X/01/130401 + 21 $35.00/0 © 2001 Academic Press

evanescent higher order modes at the discontinuity. The acoustic field must be continuous, and the plane wave propagation is not able to satisfy continuity without the presence of higher order modes. The simplicity of the plane wave propagation model, however, has led to its wide use for the prediction of the acoustic behaviour of mufflers. Of course, the analysis is valid only up to the cut-off frequency, or even to a lower value, due to the loss in accuracy that can be produced by the presence of evanescent modes. In order to improve the results obtained via the plane wave model and increase the frequency range of the analysis, it is possible to use other techniques, such as multi-dimensional analytical solutions of the wave equation or numerical methods.

In the first case, three approaches have been found to be commonly used, which differ in the representation of the duct discontinuities. These are: the point source method [1], the piston-driven model [2–4] and the mode-matching technique [5]. The simplest and most inaccurate one is the point source method, since the inlet and outlet pipes are not considered in the analysis. These ports are substituted by a point that represents the flow source. This assumption is acceptable when the dimensions of the ports are sufficiently small compared with the size of the muffler and the smallest wavelength of interest. The piston-driven model takes into account the discontinuities in the inlet and outlet ports by using the averaged pressures, whence results better than those obtained from the point source method should be expected. The mode-matching technique is the most exact analytical method, since it considers wave propagation in the whole domain (chamber and pipes), and it is based on the continuity conditions of the acoustic field, but its major disadvantage comes from the associated mathematical complexities. Any of these techniques can be useful for high-frequency analysis, enabling the frequency range to be extended beyond the plane wave limit, having important advantages such as the computational requirements compared with other numerical methods. Their most important drawbacks, however, are the geometrical limitations. The analytical solutions of the wave equation are available only for a few simple geometries, namely rectangular, circular and elliptical ducts, but fortunately these are widely used in noise control. As far as the circular case is concerned, many researchers have obtained analytical solutions for its acoustic performance, proposing ideas which are also useful for the elliptical case. Kim and Soedel [1] applied the point source method combined with modal superposition to obtain the four-pole parameters of three-dimensional cavities. Ih and Lee [2] studied the performance of an offset inlet/outlet expansion chamber and they included the effect of a uniform mean flow. These authors used the piston-driven model and evaluated the four-pole parameters, and good agreement with experimental results was found in general. Following the previous procedure, Ih and Lee [3] also investigated the behaviour of the reversing chamber muffler. Kim and Choi [4] considered a reversing chamber muffler with a temperature gradient, dividing the geometry into a number of segments with a constant temperature. They applied the piston-driven model to take into account the inlet and outlet ports, and the mode-matching technique to relate the pressure and velocity fields between segments. Åbom [5] applied the mode-matching technique and obtained the four-pole parameters in extended inlet/outlet expansion chambers, considering the propagation of higher order modes. His results showed good agreement with experimental measurements and the results from reference [2]. Selamet and Radavich [6] also adopted a similar technique in order to study the effect of length on the acoustic behaviour of expansion chambers. They studied the whole domain, that is, including wave propagation in the inlet and outlet ducts (this is not taken into account when the point source method or piston-driven model are applied). These authors used the continuity condition of acoustic pressure and axial velocity to obtain an infinite set of equations that provides the coefficients of the waves in the ducts. The length-to-diameter ratio was found to be quite

important in the acoustic behaviour. When it is higher than 0·41, one-dimensional domes are obtained in the transmission loss. When it is lower, a resonance behaviour with peaks below the onset of any multi-dimensional mode is found to appear. Selamet and Ji [7] and Selamet *et al.* [8] also studied the performance of circular expansion chambers with offset inlet/outlet and obtained the transmission loss for a number of geometries with different length, offset distance and relative angle. They compared their results with boundary element solutions, obtaining good agreement. The effect of the geometry on the three-dimensional propagation was shown to be very important, since the propagation of higher order modes can be eliminated by means of varying the relative location of the inlet and outlet pipes. The acoustic behaviour of the reversing chamber was studied in detail in reference [9], using the mode-matching technique. As will be shown, some of the trends found in circular chambers are quite similar to those that appear in the elliptic case. Recently, Selamet and Ji [10] have considered the acoustic behaviour of expansion chambers with extended inlet/outlet. An analytical mode-matching model is presented for the concentric geometry. It is shown that a suitable selection of the extended lengths can lead to an excellent acoustic performance. All these analytical contributions are applied to circular chambers, and so they are based on the use of Bessel functions and their properties. In the case of the elliptical geometry, a few references have been found that deal with analytical solutions, most of them applied to the propagation of electromagnetic fields in waveguides [11–13]. Other related papers dealt with the problem of flexural vibrations of elliptical plates [14, 15]. In the case of the acoustic problem, Hong and Kim [16] considered hollow and annular elliptical cavities and obtained the natural frequencies and mode shapes by means of the Mathieu functions. This paper is the starting point of the work presented here.

In the case of numerical techniques, the boundary element method and the finite element method (FEM) are the most interesting ones (see references [17, 18]). One of their major advantages is the possibility to analyze problems with arbitrary geometry and general boundary conditions, but at the cost of long computation times if sufficient accuracy is desired at high frequencies, due to the large number of elements required.

In the present paper, the problem of wave propagation in elliptical chamber mufflers is considered from several points of view. The solution of the wave equation in elliptic co-ordinates is expressed in terms of the Mathieu functions, obtaining the natural frequencies and mode shapes. The modal superposition technique and the point source method have been applied to a number of elliptical mufflers (expansion chambers and reversing chambers) to obtain their transmission loss. The results are compared with those obtained from the finite element method and from experiments, showing a good agreement. Polynomial fitting curves have been evaluated to enable the prediction of the cut-off frequency in concentric and non-concentric elliptical chambers, as well as the optimum location of the outlet, as a function of the eccentricity and the dimensions. Finally, the influence of the geometry on the acoustic behaviour and the propagation of higher order elliptic modes is studied.

2. ANALYTICAL MODEL

In Figure 1, the cross-section of an elliptical chamber is depicted, showing both Cartesian and elliptic co-ordinate systems. The relationship between these two sets of co-ordinates is given by [16, 19]

$$x = \rho \cosh u \cos v, \qquad y = \rho \sinh u \sin v, \qquad z = z. \tag{1–3}$$

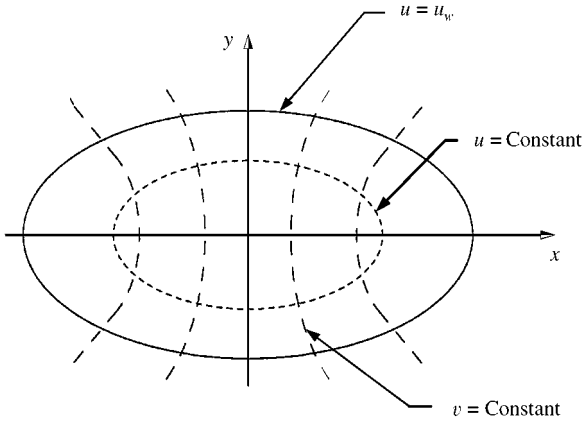

Figure 1. Elliptical cross-section.

Here, ρ is half the distance between the ellipse focii. The wave propagation in a three-dimensional domain is governed by the wave equation [20]

$$\nabla^2 p - \frac{1}{c_0^2}\frac{\partial^2 p}{\partial t^2} = 0, \tag{4}$$

where p is the acoustic pressure, c_0 is the speed of sound and t is the time variable. Using elliptic co-ordinates and setting $p = P\mathrm{e}^{\mathrm{j}\omega t}$, where P is the pressure complex amplitude, ω is the angular frequency and $\mathrm{j} = \sqrt{-1}$, gives

$$\frac{\partial^2 P}{\partial z^2} + \frac{2}{\rho^2(\cosh 2u - \cos 2v)}\left(\frac{\partial^2 P}{\partial u^2} + \frac{\partial^2 P}{\partial v^2}\right) + k^2 P = 0, \tag{5}$$

where $k = \omega/c_0$ is the wavenumber.

2.1. NATURAL FREQUENCIES AND MODE SHAPES IN ELLIPTIC CO-ORDINATES

Equation (5) is solved applying the method of separation of variables and the rigid wall boundary conditions [16], giving the mode shapes as

$$P^{\mathrm{even}}_{r,n,i}(u, v, z) = \mathrm{ce}_r(v, q_{r,i})\,\mathrm{Ce}_r(u, q_{r,i})\cos(n\pi z/L) \tag{6}$$

for $r = 0, 1, 2, \ldots, n = 0, 1, 2, \ldots,$ and $i = 1, 2, \ldots,$ and

$$P^{\mathrm{odd}}_{r,n,i}(u, v, z) = \mathrm{se}_r(v, \bar{q}_{r,i})\,\mathrm{Se}_r(u, \bar{q}_{r,i})\cos(n\pi z/L) \tag{7}$$

for $r = 1, 2, \ldots, n = 0, 1, 2, \ldots,$ and $i = 1, 2, \ldots$.

Here, $\mathrm{ce}_r(v, q)$, $r = 0, 1, 2, \ldots,$ (even solutions), and $\mathrm{se}_r(v, \bar{q})$, $r = 1, 2, \ldots,$ (odd solutions), are Mathieu functions of the first kind and order r, whereas $\mathrm{Ce}_r(u, q)$, $r = 0, 1, 2, \ldots,$ (even solutions), and $\mathrm{Se}_r(u, \bar{q})$, $r = 1, 2, \ldots,$ (odd solutions) are modified Mathieu functions of the first kind, and L is the chamber length. The terms q (for even solutions) and $\bar{q}$ (for odd solutions) are referred to as parameter of Mathieu equations, related with a separation constant C, ρ and k by means of

$$(k^2 - C^2)\,\rho^2/2 = 2q. \tag{8}$$

Finally, the associated angular frequency is given by

$$\omega = c_0 \sqrt{4q/\rho^2 + (n\pi/L)^2} \tag{9}$$

for even solutions ($\bar{\omega}$ will be used for the odd ones). These mode shapes are used in the next section to evaluate the frequency response functions of a given chamber.

2.2. EVALUATION OF THE FREQUENCY RESPONSE FUNCTIONS

The acoustic response of the elliptical chamber may be obtained, once the mode shapes are known, by means of modal superposition [1]. Assuming harmonic behaviour, the relationship between the acoustic variables in the inlet and outlet of the chamber is given by its four-pole parameters [20]

$$\begin{bmatrix} P_1 \\ U_1 \end{bmatrix} = \begin{bmatrix} A & B \\ C & D \end{bmatrix} \begin{bmatrix} P_2 \\ U_2 \end{bmatrix}, \tag{10}$$

where subscripts 1 and 2 refer to the inlet and outlet, respectively, and P and U denote the acoustic pressure and velocity complex amplitudes. The pressure at any point can be written as a linear combination of the velocity at the inlet and outlet. This means that

$$\begin{bmatrix} P_1 \\ P_2 \end{bmatrix} = \begin{bmatrix} H_{11} & H_{12} \\ H_{21} & H_{22} \end{bmatrix} \begin{bmatrix} U_1 \\ -U_2 \end{bmatrix}, \tag{11}$$

where H_{ij} represents the frequency response function, defined as the pressure response at co-ordinate i due to a velocity excitation at co-ordinate j. Both representations completely define the muffler, and it is therefore possible to obtain equation (10) from equation (11) and *vice versa*. The four-pole parameters can then be written as

$$A = \frac{H_{11}}{H_{21}}, \qquad B = -H_{12} + \frac{H_{11}\,H_{22}}{H_{21}}, \qquad C = \frac{1}{H_{21}}, \qquad D = \frac{H_{22}}{H_{21}}, \tag{12–15}$$

from which the transmission loss can be evaluated [20].

The frequency response functions are calculated considering the non-homogeneous wave equation, which includes an excitation source [1]

$$\nabla^2 p - \frac{1}{c_0^2}\frac{\partial^2 p}{\partial t^2} = -\frac{\partial \dot{m}(u, v, z, t)}{\partial t}, \tag{16}$$

where $\dot{m}$ is the function that defined the mass flow coming into the chamber. Assuming that point source conditions hold, the pressure response, that is, the frequency response function at the point (u, v, z) with respect to an excitation applied at (u^1, v^1, z^1), is obtained [1] as

$$\frac{P(u, v, z)}{U_1} = \mathrm{j}\omega\rho_0 S_1 c_0^2 \left(\sum_{r=0}^{\infty}\sum_{n=0}^{\infty}\sum_{i=1}^{\infty} \frac{P^{\text{even}}_{r,n,i}\,(u, v, z)\;P^{\text{even}}_{r,n,i}\,(u^1, v^1, z^1)}{N^{\text{even}}_{r,n,i}\,(\omega^2_{r,n,i} - \omega^2)} + \sum_{r=1}^{\infty}\sum_{n=0}^{\infty}\sum_{i=1}^{\infty} \frac{P^{\text{odd}}_{r,n,i}\,(u, v, z)\;P^{\text{odd}}_{r,n,i}\,(u^1, v^1, z^1)}{N^{\text{odd}}_{r,n,i}\,(\bar{\omega}^2_{r,n,i} - \omega^2)} \right), \tag{17}$$

where ρ_0 is the fluid density, S_1 is the cross-section in which the excitation is applied (in this case the inlet cross-section), U_1 is the acoustic velocity complex amplitude of excitation, V is the volume of the domain, $N^{\text{even}}_{r,n,i} = \int_V P^{\text{even}}_{r,n,i}\,(u, v, z)^2\,\mathrm{d}V$ and $N^{\text{odd}}_{r,n,i} = \int_V P^{\text{odd}}_{r,n,i}\,(u, v, z)^2\,\mathrm{d}V$.

3. COMPARISON WITH MEASUREMENTS AND FEM RESULTS

In order to validate the previous theoretical developments, comparison between the results obtained, measurements and numerical calculations will now be presented. The magnitude used for comparison purposes is the transmission loss (TL), as usual. Explicit comparison will be presented with experimental measurements performed with a modified impulse method [21], and with finite element results, for two cases of interest: a concentric chamber and a reversing chamber.

Figure 2 shows a concentric expansion chamber. As can be seen, it is symmetric about both axes of the ellipse. This implies that only those modes that share the same symmetry may propagate. Odd modes do not propagate since they are not symmetric about the major axis of the ellipse, and among the even modes only those of the $(2r, i)$ order, with $r = 0, 1, 2, \ldots$ and $i = 1, 2, \ldots,$ may propagate, due to the fact that the even modes of $(2r + 1, i)$ order are not symmetric about the minor axis. Then, the frequency response functions are obtained retaining the propagating even terms in equation (17), setting the co-ordinates of the inlet point to $u^1 = 0$, $v^1 = \pi/2$ and $z^1 = 0$, and those of the outlet point to $u^2 = 0$, $v^2 = \pi/2$ and $z^2 = L$. A concentric chamber with major semi-axis $a = 0{\cdot}23/2$ m, minor semi-axis $b = 0{\cdot}13/2$ m, eccentricity $\varepsilon = (1 - b^2/a^2)^{1/2} = 0{\cdot}8249$ and semi-interfocal distance $\rho = \varepsilon a = 0{\cdot}0948$ m has been chosen. The inlet and outlet radii, R_1 and R_2, are equal to $0{\cdot}033/2$ m. In Table 1, the numerical values of the natural frequencies associated with

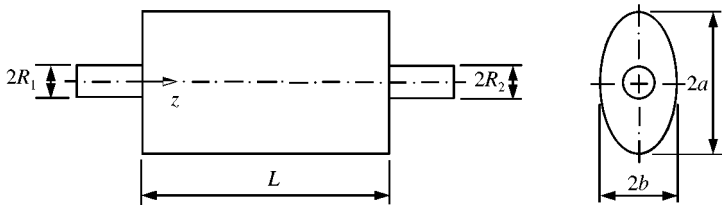

Figure 2. Concentric expansion chamber.

TABLE 1

Natural frequencies of transversal modes for $a = 0{\cdot}23/2$ *and* $b = 0{\cdot}13/2$ m

Even mode	q parameter	f(Hz)
(0, 1)	0·0	0·0
(0, 2)	6·201	2840·886
(0, 3)	22·987	5469·529
(1, 1)	0·595	880·002
(1, 2)	8·758	3375·984
(1, 3)	27·555	5988·356
(2, 1)	1·965	1599·213
(2, 2)	11·967	3946·369
(2, 3)	32·722	6525·741
(3, 1)	4·058	2297·985
(3, 2)	15·887	4547·053
(3, 3)	38·515	7079·831
(4, 1)	6·837	2982·855
(4, 2)	20·565	5173·364
(4, 3)	44·957	7649·012

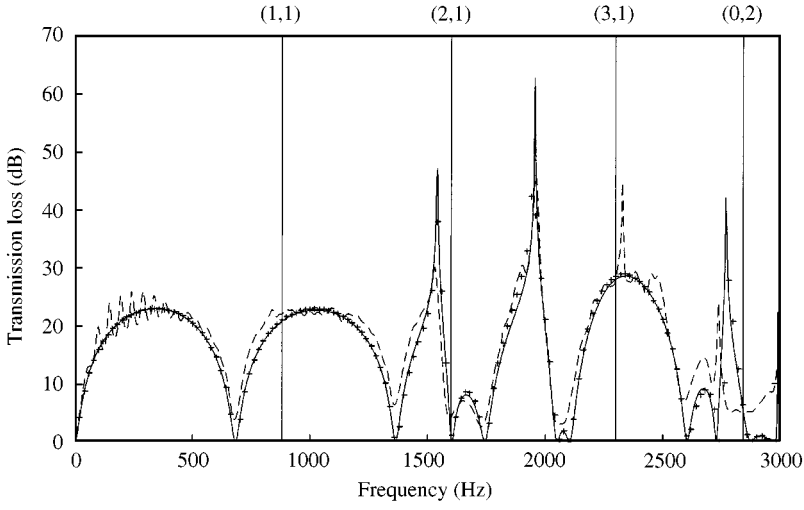

Figure 3. Transmission loss of concentric expansion chamber with $a = 0{\cdot}23/2$ m, $b = 0{\cdot}13/2$ m, $R_1 = R_2 = 0{\cdot}033/2$ m and $L = 0{\cdot}25$ m: ——, analytical; – – –, experimental; +, finite elements.

some of the transversal modes of the chamber are shown. As mentioned before, only the even modes of the $(2r, i)$ order may propagate due to symmetry reasons. This can be clearly appreciated in Figure 3, in which the transmission loss is shown. The agreement observed between the measurement, the finite element result and the analytical prediction is acceptable, all the more if one considers the complex shape of the curves for frequencies above the range of pure plane wave propagation. This shape is determined by the onset and/or propagation of transversal modes and their combinations with axial modes. Transversal modes, whose position is indicated in the Figure, will be taken as reference for comparison purposes. The first transversal mode to propagate is mode (2, 1), as indicated by the typical collapse of the transmission loss at the associated frequency. Next, the onset of mode (0, 2) can be observed, being the last one to appear in the frequency range represented. It is worth noticing that the measurements exhibit spikes at frequencies corresponding to modes which cannot propagate; one such spike can be found near the cut-off frequency of the (1, 1) mode, but the most evident case appears at the cut-off frequency of the (3, 1) mode. This should be attributed to the fact that the chamber used in the tests is not perfectly concentric. The deviations between the measurement and both theoretical results for frequencies above 2500 Hz may be justified by this fact, in addition to the neglected viscous effects. There are also some deviations and oscillations in the experimental result before multi-dimensional propagation that seem to be associated with weak non-linearities due to the pressure amplitude used in the impulse test [21].

For the case of the reversing chamber, the geometry considered is depicted in Figure 4. The centres of the inlet and outlet sections are located on the major axis of the ellipse, so that the chamber is symmetric about that axis. Only those modes that are symmetric with respect to that axis will propagate, namely, all the even modes. The elliptical cross-section is the same as for the concentric chamber discussed above, and thus the list of modes is that shown in Table 1. The inlet and outlet radii, R_1 and R_2, are equal to $0{\cdot}051/2$ m. Now the co-ordinates of the inlet point are $u^1 = 0$, $v^1 = \arccos(\delta_1/\rho)$ and $z = 0$, and for the outlet point one has $u^2 = 0$, $v^2 = \arccos(\delta_2/\rho)$ and $z^2 = 0$ (the offset distances are less than the semi-interfocal distance ρ). In the configuration chosen (centred inlet), the distance between the ducts is relatively small; hence, providing a test for the point source assumption. As it

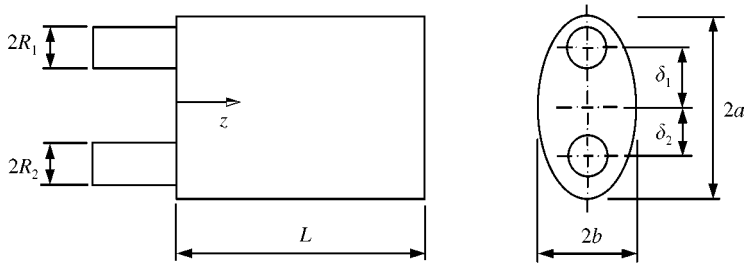

Figure 4. Reversing chamber.

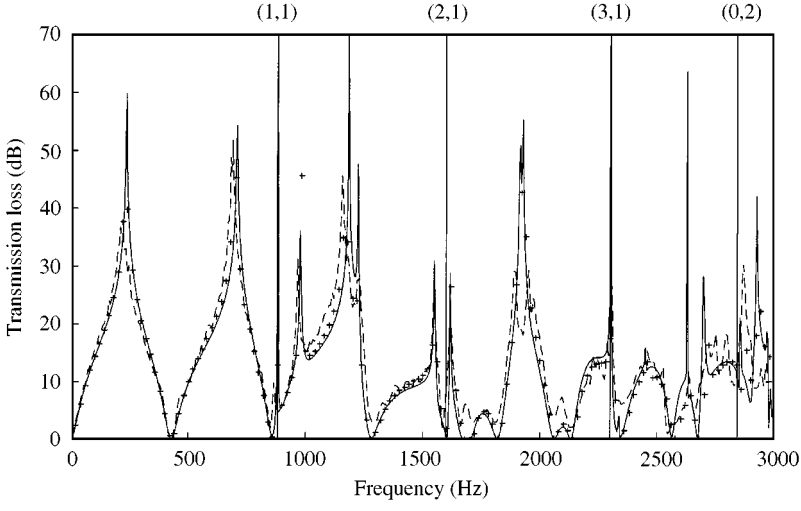

Figure 5. Transmission loss of reversing chamber with $a = 0{\cdot}23/2$ m, $b = 0{\cdot}13/2$ m, $R_1 = R_2 = 0{\cdot}051/2$ m, $\delta_1 = 0$ m, $\delta_2 = 0{\cdot}073$ m and $L = 0{\cdot}4$ m: ——, analytical; – – –, experimental; +, finite elements.

will be seen in a following section, this particular case of centred inlet eliminates the propagation of the even modes of the $(2r + 1, i)$ order. The corresponding results are shown in Figure 5, where the agreement is in general good, with an acceptable reproduction of the main features found in the experimental curve. Now, all the even modes of the $(2r, i)$ order propagate, and those of the $(2r + 1, i)$ order do not (centred inlet), as indicated by the corresponding collapses in the transmission loss.

As a conclusion, it may be stated that, for the purposes of the present work, the point source representation gives a sufficient approximation to the physics of the problem, at least for those cases in which the length of the chamber and the dimensions of the cross-section are large enough in comparison with the diameters of the inlet and outlet.

4. DETERMINATION OF THE FIRST CUT-OFF FREQUENCY

As mentioned before, the plane wave model is valid only below the frequency corresponding to the first transversal mode (cut-off frequency) since above this frequency transversal modes propagate without attenuation. Moreover, even below the cut-off frequency the plane wave model can lead to incorrect results, mainly in the vicinity of

singularities, in which evanescent modes appear. Therefore, it is imperative to determine the value of this cut-off frequency. In the case of circular ducts, this may be easily obtained in terms of the zeros of the Bessel functions [20]. If circumferential modes may propagate (circular chambers with non-concentric inlet and/or outlet) the cut-off frequency is

$$f_c = 1{\cdot}84c_0/(2\pi R), \tag{18}$$

where R is the chamber radius. If only radial modes may propagate (concentric inlet and outlet) the expression is

$$f_c = 3{\cdot}83c_0/(2\pi R), \tag{19}$$

so that the validity range for the plane wave model extends to more than double the limit given by equation (18). In any case, the only relevant parameter is the radius. In the elliptic geometry, however, the dependence is somewhat more complex, the two relevant parameters being now a characteristic length such as ρ and the eccentricity ε.

In the case of concentric chambers, these are symmetric about the two axes of the ellipse, so only even modes of the order $(2r, i)$, with $r = 0, 1, 2, \ldots$, and $i = 1, 2, \ldots$, may propagate. It is thus necessary to determine which of them is associated with a lower frequency. For the even modes (0, 2) and (2, 1) (see Figures 6 and 7), the values of the parameters $q_{0,2}$ and $q_{2,1}$ may be obtained as a function of eccentricity from the rigid wall boundary condition, the results being shown in Figure 8. It can be confirmed that $q_{2,1}$ is always below $q_{0,2}$. When the eccentricity tends to zero, this reverts to the circular case so that $(q_{0,2}/q_{2,1})^{1/2}$ tends to $3{\cdot}83/3{\cdot}05$ [20]. For instance, if one considers an eccentricity $\varepsilon = 0{\cdot}02$, the value $(q_{0,2}/q_{2,1})^{1/2} = (0{\cdot}001468/0{\cdot}000933)^{1/2} = 1{\cdot}2543$ is obtained, and thus the (2, 1) mode is the first one to propagate. The cut-off frequency is obtained from equation (9) as

$$f_c = (c_0/2\pi)\sqrt{4q_{2,1}(\varepsilon)/\rho^2}. \tag{20}$$

In view of the complexity of the Mathieu functions, for the corresponding cut-off frequency, a sixth degree polynomial has been fitted to the value $f_c\rho/c_0$, giving

$$(f_c\rho/c_0)_{2,1} = -1{\cdot}2285\times10^{-4} + 0{\cdot}4895\varepsilon - 0{\cdot}0284\varepsilon^2 + 0{\cdot}2098\varepsilon^3 - 0{\cdot}0781\varepsilon^4 - 0{\cdot}1172\varepsilon^5 + 0{\cdot}0794\varepsilon^6, \tag{21}$$

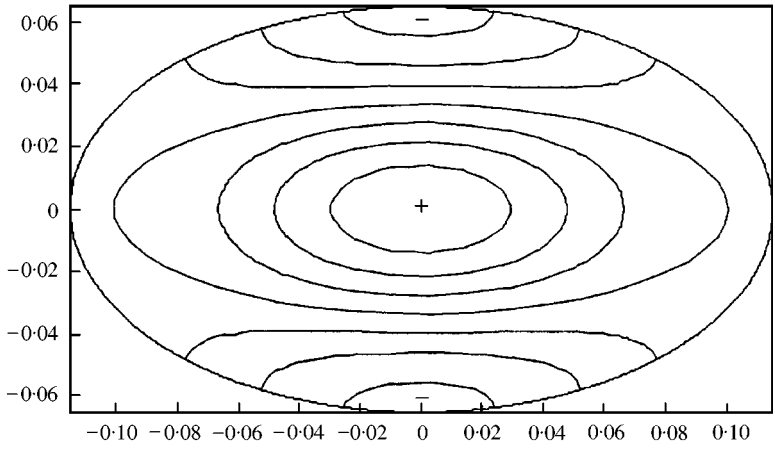

Figure 6. Even mode shape (0, 2).

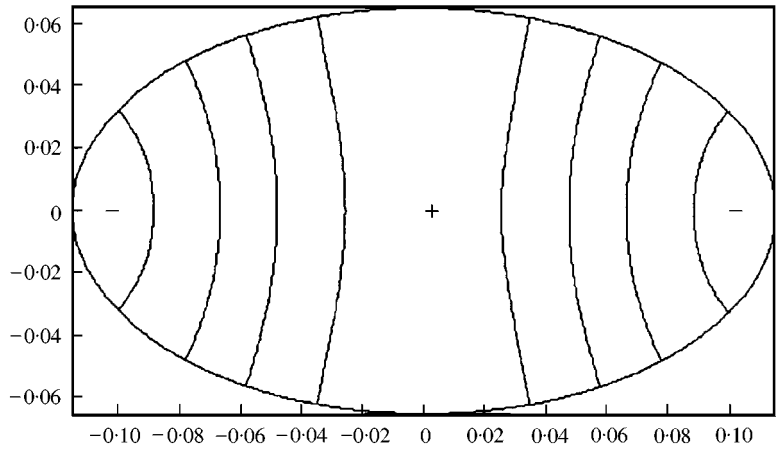

Figure 7. Even mode shape (2, 1).

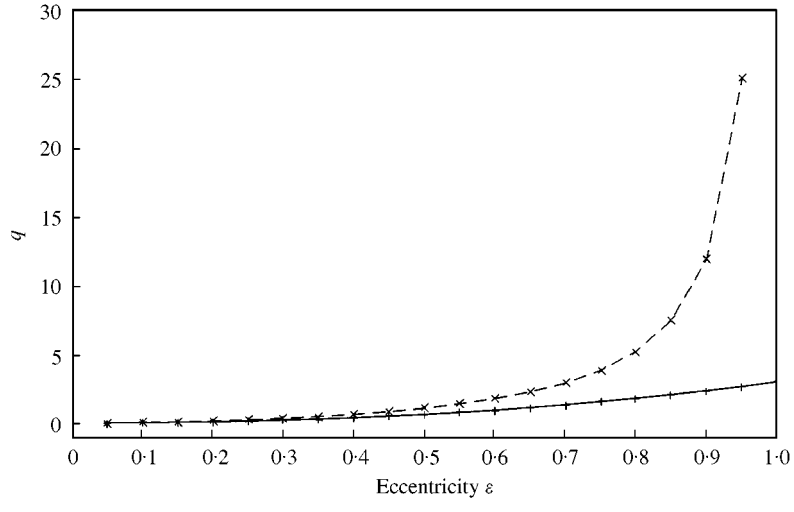

Figure 8. Parameters $q_{0,2}$ and $q_{2,1}$ as a function of eccentricity ε: —×—×—, $q_{0,2}$; $-+-+-$, $q_{2,1}$.

valid for eccentricities $\varepsilon > 0{\cdot}05$. For instance, the dimensions of one of the chambers considered in this work are $a = 0{\cdot}23/2$ and $b = 0{\cdot}13/2$ m ($\varepsilon = 0{\cdot}8249$ and $\rho = 0{\cdot}0948$ m). The cut-off frequency obtained from equation (21) is $f_c = 1599{\cdot}28$ Hz, while the exact value is 1599.21 Hz. If the value $a = 0{\cdot}23/2$ m is kept constant and the eccentricity decreases, equation (21) gives a cut-off frequency of 1437·39 Hz for $\varepsilon = 0{\cdot}05$, which tends to the theoretically expected cut-off frequency of 1435·16 Hz for a cylinder of radius a (mode $m = 2$, $n = 0$ [20]). In the case of the offset inlet/outlet expansion chambers and reversing chamber mufflers, where the centre of the inlet and outlet pipes are located in the major axis, all the even modes may propagate, since they are symmetric about this axis. The first even mode to propagate is the mode (1, 1) (see Figure 9). Again, a sixth order polynomial was fitted to the results obtained for $f_c\rho/c_0$, the expression begin now

$$(f_c\rho/c_0)_{1,1} = 7{\cdot}0771 \times 10^{-7} + 0{\cdot}293\,\varepsilon + 2{\cdot}1415 \times 10^{-4}\,\varepsilon^2 + 0{\cdot}005\,\varepsilon^3 + 0{\cdot}0021\,\varepsilon^4 - 0{\cdot}0013\,\varepsilon^5 + 0{\cdot}0012\,\varepsilon^6, \tag{22}$$

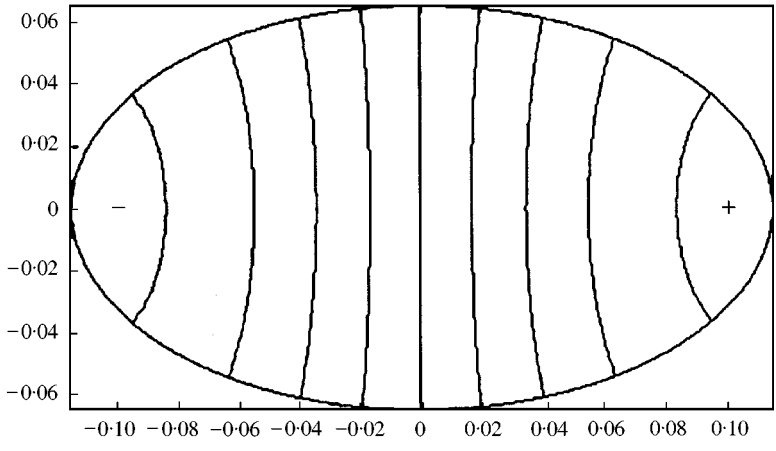

Figure 9. Even mode shape (1, 1).

valid for eccentricities $\varepsilon > 0{\cdot}05$. For example, with the same dimensions considered before, the cut-off frequency obtained from equation (22) is $f_c = 880{\cdot}005$ Hz, whereas the exact value is 880·002 Hz. If the value of a is kept constant to 0·23/2 m, setting $\varepsilon = 0{\cdot}05$ in equation (22) gives a cut-off frequency of 866·4 Hz, which tends to the theoretically expected cut-off frequency of 865·8 Hz for a cylinder of radius a (mode $m = 1$, $n = 0$ [20]).

5. DETERMINATION OF THE NODAL LINE FOR THE MODE (2, 1)

As it has been shown [2, 8, 9] for circular chambers, by centering the inlet and offsetting the outlet appropriately (towards the pressure nodal line of the first radial mode, which is located at a distance of 0·6276 times the radius of the chamber from the centre), the acoustic attenuation performance can be improved. This idea can be easily extended to the case of elliptical geometries. The propagation of the elliptic mode (1, 1) can be eliminated by locating the inlet in the centre of the chamber, since this point is contained in the nodal line. Now, the question deals with the propagation of the following transversal mode, in that case the mode (2, 1). In Figure 7, the nodal lines can be seen to be confocal hyperbolas. Since the chambers considered have their inlet and outlet located in the major axis of the ellipse, the intersection of this axis and the nodal line will provide the required point to allocate the outlet if the propagation of mode (2, 1) is intended to be suppressed. This point is always contained in the focal line ($u = 0$), so its position in the major axis is given by equation (1), and yields

$$x_c = \rho \cos v_c, \tag{23}$$

where x_c is the offset distance of the nodal line and v_c is the corresponding elliptic co-ordinate. The value of the offset distance depends on some characteristic length, such as the semi-interfocal distance ρ, and the eccentricity ε. In order to obtain an easy evaluation of the nodal line location, a sixth-degree polynomial has been fitted to the value v_c, giving

$$v_c = 0{\cdot}7851 + 0{\cdot}0076\,\varepsilon + 0{\cdot}3502\,\varepsilon^2 - 0{\cdot}0533\,\varepsilon^3 + 0{\cdot}9358\,\varepsilon^4 - 1{\cdot}5667\,\varepsilon^5 + 0{\cdot}6556\,\varepsilon^6, \tag{24}$$

valid for eccentricities $\varepsilon > 0{\cdot}05$. For the same dimensions as in the examples of section 4, a value $v_c = 1{\cdot}0412$ is obtained from equation (24) (the exact value is 1·0411). Equation (23)

gives the offset distance $x_c = 0{\cdot}0479$ m. The effects of this offset in the acoustic performance of the elliptical chamber will be discussed in detail in the following section.

6. RESULTS AND DISCUSSION

The analytical model based on Mathieu functions and modal superposition, as well as finite element calculations, will be used to study the effect of some relevant parameters in the acoustic behaviour of mufflers with elliptical cross-section. As in the case of circular chambers (see references [8, 9]), the length of the chamber and the relative location of the inlet/outlet have to be considered. In addition, the eccentricity of the chamber has been found to play an important role in the acoustic attenuation performance. The analysis is applied to expansion chambers and reversing chambers with the inlet and outlet located in the major axis of the ellipse. In all the cases considered, the cross-section of the chambers is kept constant. Two eccentricities are taken into account: the first one has a high value, $\varepsilon_1 = 0{\cdot}8249$ (semi-axes $a = 0{\cdot}23/2$ and $b = 0{\cdot}13/2$ m), and its transversal natural frequencies were shown in Table 1. The second one has a lower value, $\varepsilon_2 = 0{\cdot}3$ (semi-axes $a = 0{\cdot}177/2$ and $b = 0{\cdot}1688/2$ m), and the natural frequencies can be seen in Table 2. In addition, a circular chamber is included in the analysis (with a equivalent radius $r_{eq} = 0{\cdot}1728/2$ m), whose TL has been obtained via the method developed by Selamet and Radavich [6] and Selamet and Ji [9]. In all the configurations, the inlet and outlet radii are $R_1 = R_2 = 0{\cdot}033/2$ m.

6.1. EXPANSION CHAMBERS

Figure 10 shows the transmission loss for concentric expansion chambers with $L = 0{\cdot}25$ m and eccentricities ε_1 and ε_2. In addition, the TL of a circular expansion chamber (with r_{eq}) is also depicted. The transmission loss for the elliptical geometry has been

TABLE 2

Natural frequencies of transversal modes for $a = 0{\cdot}177/2$ *and* $b = 0{\cdot}1688/2$ m

Even mode	q parameter	f(Hz)
(0, 1)	0·0	0·0
(0, 2)	0·348	2403·077
(0, 3)	1·175	4417·896
(1, 1)	0·076	1127·623
(1, 2)	0·655	3298·178
(1, 3)	1·687	5293·953
(2, 1)	0·219	1907·617
(2, 2)	1·05	4175·632
(2, 3)	2·308	6190·981
(3, 1)	0·416	2627·585
(3, 2)	1·509	5007·095
(3, 3)	3·012	7072·859
(4, 1)	0·666	3326·249
(4, 2)	2·027	5803·052
(4, 3)	3·777	7920·826

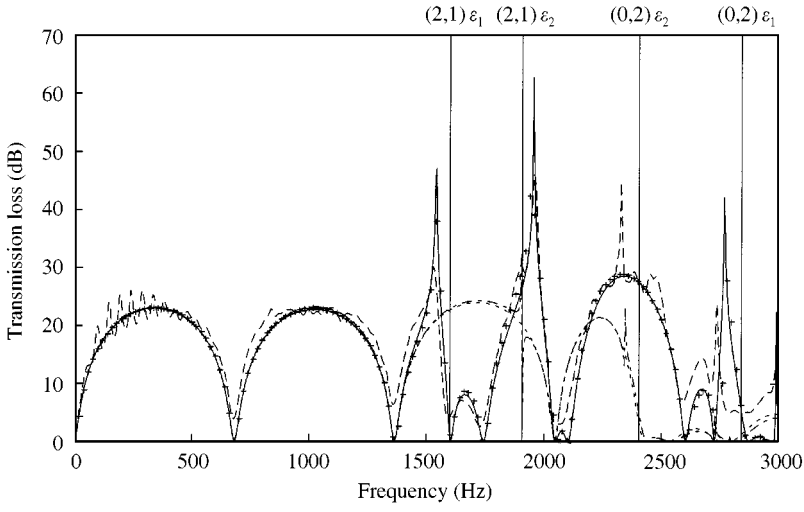

Figure 10. Transmission loss of concentric expansion chamber with $L = 0{\cdot}25$ m; ——, analytical with ε_1 ($a = 0{\cdot}23/2$ and $b = 0{\cdot}13/2$ m); – – –, same measured experimentally; +, same with finite elements; – – – – –, analytical with ε_2 ($a = 0{\cdot}177/2$ and $b = 0{\cdot}1688/2$ m); - - -, analytical [6] for circular chamber with $r_{eq} = 0{\cdot}1728/2$ m.

obtained via the point source method and finite element calculations. In the case of the chamber with eccentricity ε_1, experimental results are also depicted. The behaviour of all the chambers is found to be almost the same below the first frequency of propagation of three-dimensional waves (mode (2, 1) for ε_1) and, as the plane wave model predicts, the TL level depends on the area ratio, which is the same for all the cases. The number of domes is the same as that obtained for long circular chambers [6], and no relevant differences are found between the curves. The first collapse in the transmission loss appears in the chamber with a higher eccentricity, in which the transversal mode (2, 1) starts to propagate, whose cut-off frequency is equal to 1599·21 Hz. Above this frequency, the propagation in this chamber is multi-dimensional, and significant differences are found in comparison with the rest of geometries (elliptical with low eccentricity ε_2 and circular). The higher the eccentricity is, the lower the cut-off frequency will be, and in that sense, the acoustic performance of the elliptical chamber is found to be worse than the associated with the circular chamber with the same cross-section, whose first radial mode appears at a cut-off frequency of 2398·74 Hz, as can be seen in the Figure. This reduction of the cut-off frequency is also confirmed by the transmission loss associated with the low eccentricity chamber but in this case the behaviour of the elliptical geometry with ε_2 is quite similar to that shown by the circular geometry. The slight differences are related to the spikes of the elliptic modes, which have negligible propagation since the geometry is very close to the circular case. As an example, one spike appears at a frequency of 1907·62 Hz due to the mode (2, 1). The final collapse appears when the mode (0, 2) starts to propagate. This is approximately for the same frequency of the first radial mode of the circular chamber.

The results obtained for a short concentric expansion chamber are shown in Figure 11. The elliptical configurations with eccentricities ε_1 and ε_2 and the circular chamber (with radius r_{eq}) have a length $L = 0{\cdot}05$ m. In addition, the plane wave model is considered for comparison purposes. The transversal dimensions in all the cases are longer than the length of the chamber. For circular cross-section, the dome behaviour breaks down when the length of the chamber is short enough so that the inequality $L/(2r_{eq}) < 0{\cdot}41$ is satisfied. The behaviour of the chambers is similar to that observed in reference [6]; that is, resonant

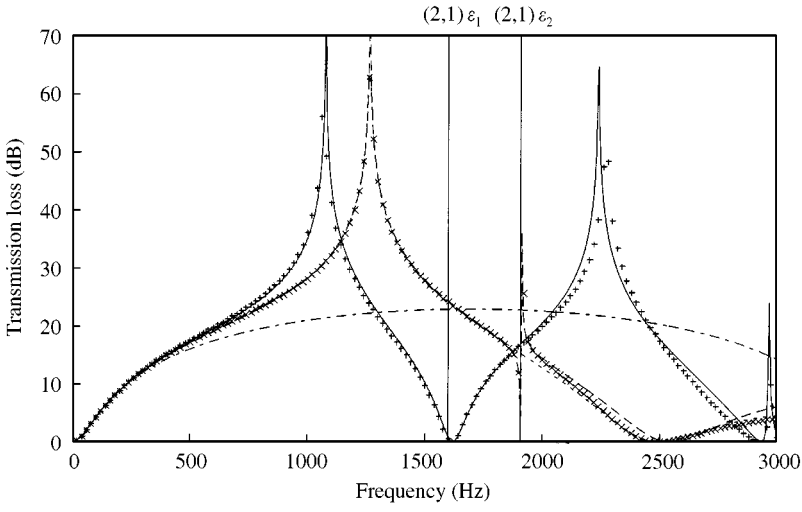

Figure 11. Transmission loss of concentric expansion chamber with $L = 0{\cdot}05$ m: ——, analytical with ε_1 ($a = 0{\cdot}23/2$ and $b = 0{\cdot}13/2$ m); +, same with finite elements; – – –, analytical with ε_2 ($a = 0{\cdot}177/2$ and $b = 0{\cdot}1688/2$ m); ×, same with finite elements; - - - -, analytical [6] for circular chamber with $r_{eq} = 0{\cdot}1728/2$ m; – – – – – plane wave model.

peaks are found at a frequency well below the onset of any higher order mode, due to the transversal propagation of the waves, and the repeating one-dimensional domes do not appear. Therefore, the plane wave model shows very little similarity with respect to the multi-dimensional results. The elliptical chamber with eccentricity ε_1 shows two peaks associated with the transversal propagation in the chamber. In this case, the assumptions of the point source method are not fully satisfied, and so some slight deviations are found in comparison with the finite element curve in the high-frequency range. The effect of the eccentricity on the reduction of the natural frequency associated with mode (2, 1) is the same as commented previously, but now the three-dimensional propagation is mainly due to the reduced length of the chamber rather than the reduction of the cut-off frequency. The transmission loss for the circular chamber and the elliptical one with eccentricity ε_2 is found to be almost the same, except the slight spikes corresponding to the elliptic modes.

An intermediate case is considered in Figure 12, in which the transmission loss is shown for $L = 0{\cdot}10$ m. The circular chamber satisfies the condition $L/(2r_{eq}) > 0{\cdot}41$, and so a well-defined one-dimensional dome is found with the first pass band at a frequency $c_0/(2L) = 1700$ Hz, the results being quite similar to those obtained by means of the plane wave model below the propagation of the mode (2, 1). The same can be said for the elliptical chamber with ε_2, whose acoustic behaviour is basically the same. However, the transversal propagation in the geometry with eccentricity ε_1 produces a peak very close to the cut-off frequency of the mode (2, 1) and there is no complete dome in the transmission loss. Now the situation is different to the case of $L = 0{\cdot}05$ m, since with this latter length all the geometries show resonant peaks in their transmission loss, but with $L = 0{\cdot}10$ m it is possible to obtain a dome behaviour or resonant peaks by changing the eccentricity. The acoustical performance of elliptical chambers is more complex than that of the circular geometry, in the sense that not only the length of the chamber but also the eccentricity have to be taken into account. Moreover, the substitution of the elliptical geometry by the circular one with the same cross-section can lead to incorrect results when the eccentricity is increased, the differences being stronger in shorter chambers, in which the transmission loss considerably differs even well below the cut-off frequency.

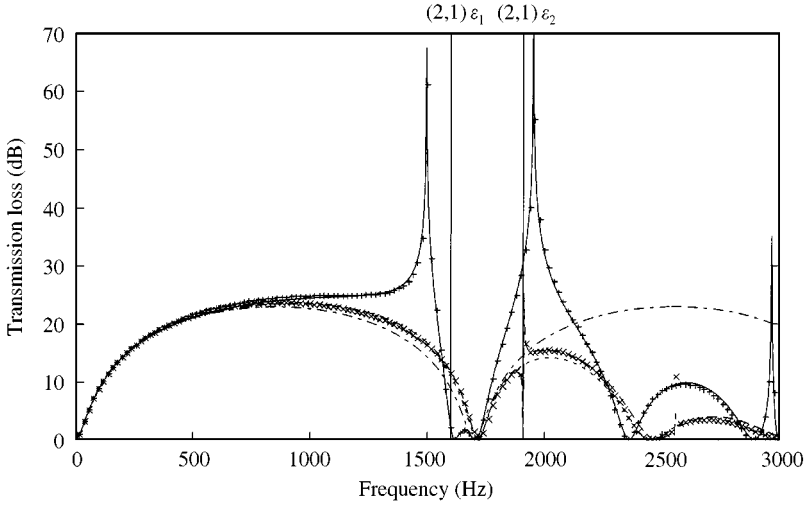

Figure 12. Transmission loss of concentric expansion chamber with $L = 0{\cdot}10$ m; ——, analytical with ε_1 ($a = 0{\cdot}23/2$ and $b = 0{\cdot}13/2$ m); +, same with finite elements; – – –, analytical with ε_2 ($a = 0{\cdot}177/2$ and $b = 0{\cdot}1688/2$ m); ×, same with finite elements; - - -, analytical [6] for circular chamber with $r_{eq} = 0{\cdot}1728/2$ m; – – – –, plane wave model.

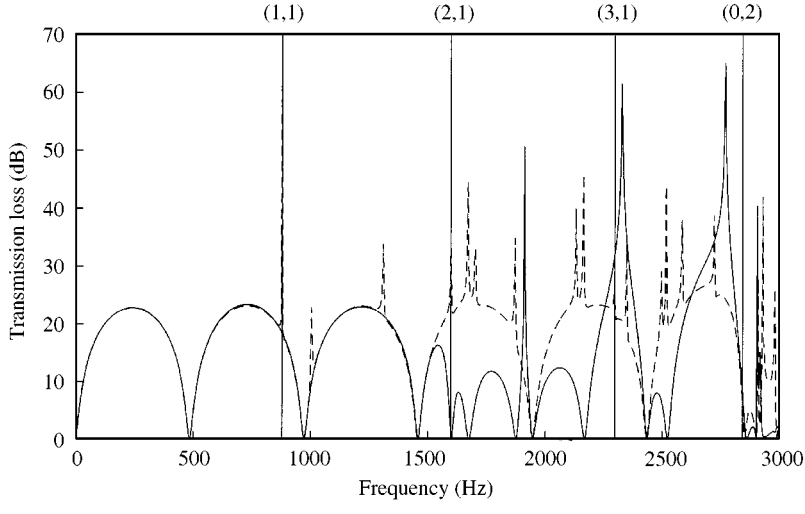

Figure 13. Analytical transmission loss of elliptical expansion chamber with $L = 0{\cdot}35$ m and eccentricity ε_1 ($a = 0{\cdot}23/2$ and $b = 0{\cdot}13/2$ m): ——, concentric chamber; – – –, centred inlet, offset outlet chamber with offset distance $x_c = 0{\cdot}0479$ m.

The effect of offsetting the outlet is now studied. As discussed earlier in the case of concentric expansion chambers, the collapse in the TL curve is due to the propagation of the mode (2, 1). This can be eliminated by a suitable offset of the outlet pipe to the corresponding nodal line, whose position was found and expressed in terms of a polynomial fitting (equation (24)). This offset allows the modes (1, 1) and (3, 1) to propagate, but this can be solved if the inlet is located at the centre of the ellipse since this point is contained in the nodal line of these modes. Figures 13–15 show the transmission loss for the elliptical chamber with eccentricity ε_1, considering the concentric and offset configurations

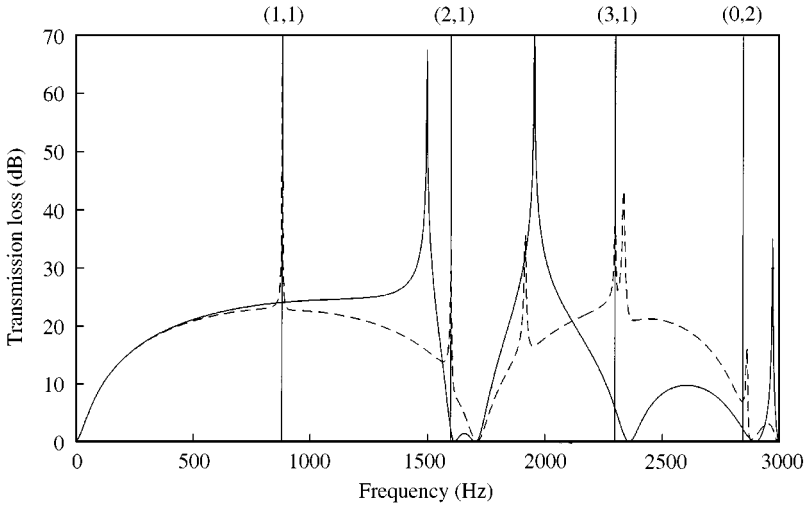

Figure 14. Analytical transmission loss of elliptical expansion chamber with $L = 0{\cdot}10$ m and eccentricity ε_1 ($a = 0{\cdot}23/2$ and $b = 0{\cdot}13/2$ m): ——, concentric chamber, – – –, centred inlet, offset outlet chamber with offset distance $x_c = 0{\cdot}0479$ m.

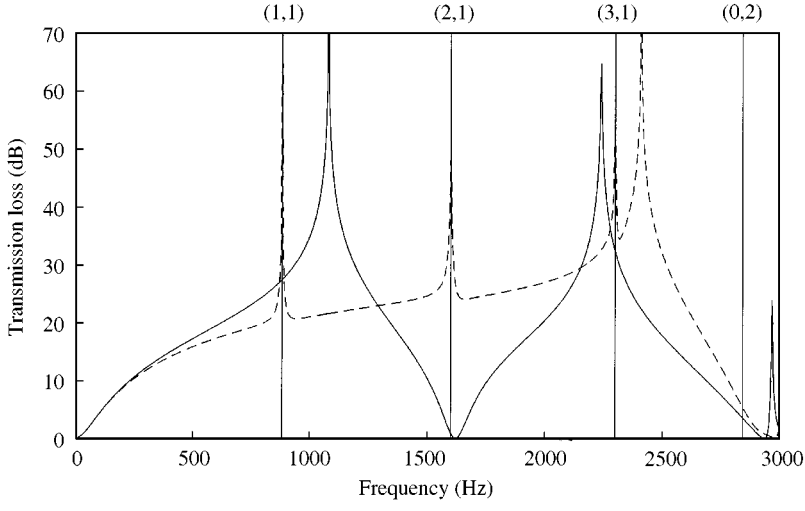

Figure 15. Analytical transmission loss of elliptical expansion chamber with $L = 0{\cdot}05$ m and eccentricity ε_1 ($a = 0{\cdot}23/2$ and $b = 0{\cdot}13/2$ m): ——, concentric chamber; – – –, centred inlet, offset outlet chamber with offset distance $x_c = 0{\cdot}0479$ m.

($x_c = 0{\cdot}0479$ m), for chamber lengths $L = 0{\cdot}35$ m, $L = 0{\cdot}10$ m and $L = 0{\cdot}05$ m respectively. The transmission loss corresponding to the longer chamber (Figure 13) is improved since the well-known behaviour of repeated domes for long chambers described in reference [6] is also found here until the collapse associated with the propagation of the mode (0, 2). In the case of the chamber with $L = 0{\cdot}10$ m (Figure 14), the transmission loss obtained with the offset also reproduces the first two domes, the pass band being associated with first pure longitudinal mode ($n = 1$, 1700 Hz). The benefits of the offset are found in the high-frequency range, but the TL is reduced from 1000 to 1600 Hz, since the transversal resonance of the mode (2, 1) is eliminated, which leads to a lower value of attenuation.

Finally, Figure 15 shows the TL for the shorter chamber whose behaviour is improved due to the fact that the pass band of the mode (2, 1) is eliminated, although the acoustic performance is worse in the frequency range from 1100 to 1200 Hz.

6.2. REVERSING CHAMBERS

Figures 16 and 17 show the transmission loss for a long reversing chamber with $L = 0{\cdot}35$ m. In both cases, the centred inlet and offset outlet configuration is considered. As can be seen in Figure 16, the centred inlet avoids the propagation of the elliptic mode (1, 1) and the well-known one-dimensional behaviour of repetitive peaks in the transmission loss appears until the onset of the mode (2, 1). The multi-dimensional analytical results and those obtained via the finite element method are shown to agree quite well. The comparison with the plane wave model reveals some differences even below the propagation of the mode (2, 1). In fact, the peaks associated with the one-dimensional resonant frequencies $(2n + 1)$ $c_0/(4L)$, $n = 0, 1, \ldots,$ are shifted with respect to the finite element and analytical results. The discrepancy is stronger than in the case of expansion chambers, since the evanescent higher order modes have more influence due to the proximity of the inlet and outlet [9]. The same comments can be applied to Figure 17, in which the low eccentricity chamber is considered analytically and numerically, as well as a circular chamber with the same cross-section. Now the cut-off frequency of 1907·62 Hz associated with the elliptic mode (2, 1) is higher than that corresponding to the high eccentricity chamber (see Figure 16), and so the range of validity of the plane wave model is increased. In fact, the transmission loss in the present case has one more peak than in the previous Figure. Some differences are found in the acoustic behaviour of reversing chambers in comparison with the simple expansion configuration. In the latter case, it has been shown that the transmission loss of the circular chamber and the ellipse with low eccentricity is similar, even when the elliptic modes start to propagate. On the contrary, if reversing chambers are considered, the low eccentricity geometry shows some differences with respect to the circular case below the first elliptic cut-off frequency, and these discrepancies become more pronounced (see Figure 17) when

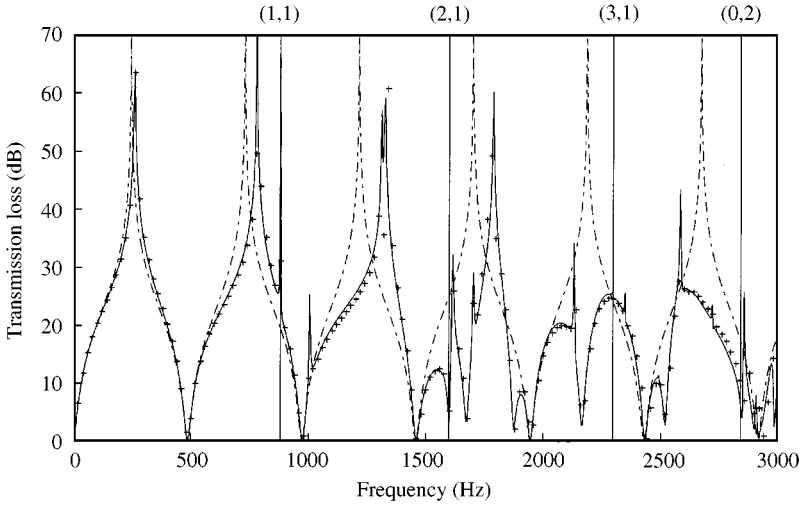

Figure 16. Transmission loss of reversing chamber with $\delta_1 = 0$ m, $\delta_2 = 0{\cdot}06$ m and $L = 0{\cdot}35$ m: ——, analytical with ε_1 ($a = 0{\cdot}23/2$ and $b = 0{\cdot}13/2$ m); +, same with finite elements; – – – –, plane wave model.

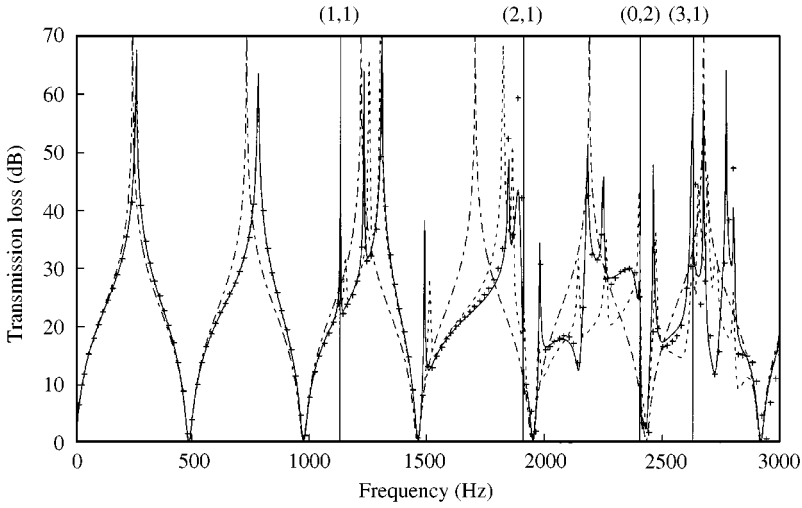

Figure 17. Transmission loss of reversing chamber with $\delta_1 = 0$ m, $\delta_2 = 0{\cdot}06$ m and $L = 0{\cdot}35$ m: ——, analytical with ε_2 ($a = 0{\cdot}177/2$ and $b = 0{\cdot}1688/2$ m); +, same with finite elements; - - -, analytical [9] for circular chamber with $r_{eq} = 0{\cdot}1728/2$ m; – – – – –, plane wave model.

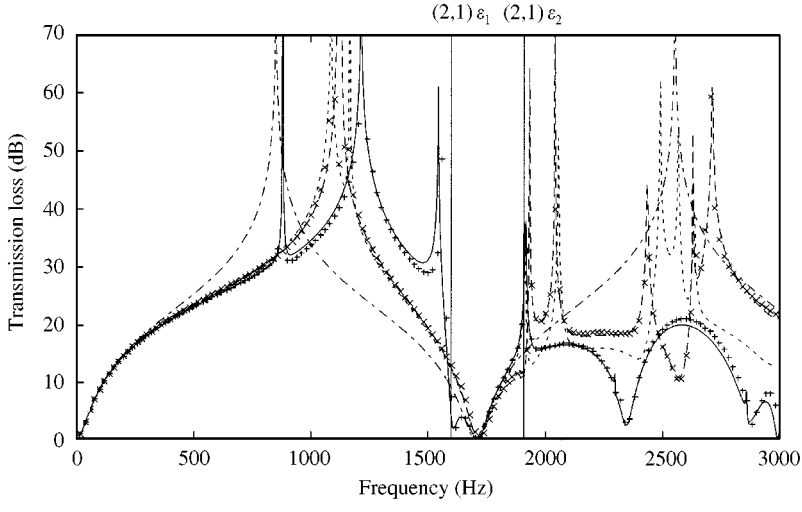

Figure 18. Transmission loss of reversing chamber with $\delta_1 = 0$ m, $\delta_2 = 0{\cdot}06$ m and $L = 0{\cdot}10$ m: ——, analytical with ε_1 ($a = 0{\cdot}23/2$ and $b = 0{\cdot}13/2$ m); +, same with finite elements; – – –, analytical with ε_2 ($a = 0{\cdot}177/2$ and $b = 0{\cdot}1688/2$ m); ×, same with finite elements; - - -, analytical [9] for circular chamber with $r_{eq} = 0{\cdot}1782/2$ m; – – – – –, plane wave model.

the elliptic modes start to propagate without attenuation. The close proximity of the inlet and outlet pipes leads to a stronger influence of the higher order modes.

These trends are also observed in Figure 18, in which the transmission loss for a short reversing chamber is depicted. The transversal propagation dominates the acoustical behaviour and so the plane wave model is able to predict the TL only for low frequencies up to 500 Hz. The first resonant peak is very close for the three geometries, circular and elliptical (with eccentricities ε_1 and ε_2), and it is located in the range from 1100 to 1200 Hz. The circular and the low eccentricity elliptic chambers have similar TL until the onset of the first elliptic mode (2, 1) at a frequency of 1907·62 Hz, which gives significant differences in

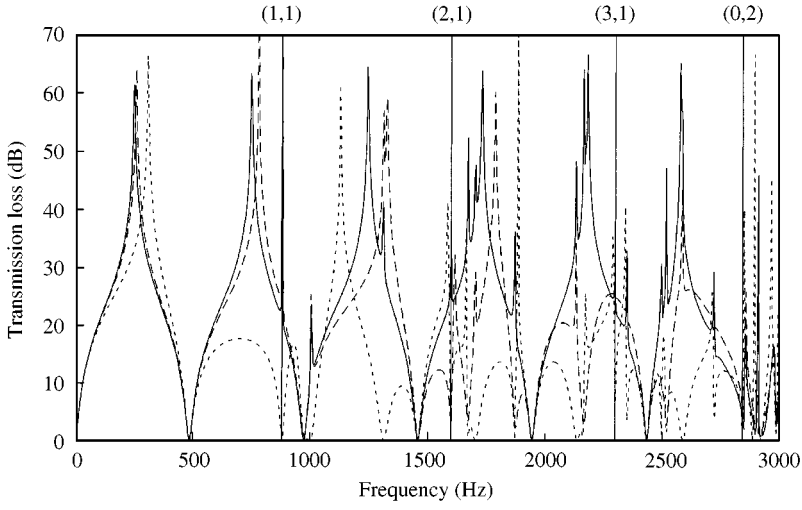

Figure 19. Analytical transmission loss of elliptical reversing chamber with $L = 0{\cdot}35$ m and eccentricity ε_1 ($a = 0{\cdot}23/2$ and $b = 0{\cdot}13/2$ m): ---, offset inlet and outlet with $\delta_1 = \delta_2 = 0{\cdot}06$ m; – – –, centred inlet, offset outlet with $\delta_2 = 0{\cdot}06$ m; ——, centred inlet, offset outlet with $\delta_2 = 0{\cdot}0479$ m.

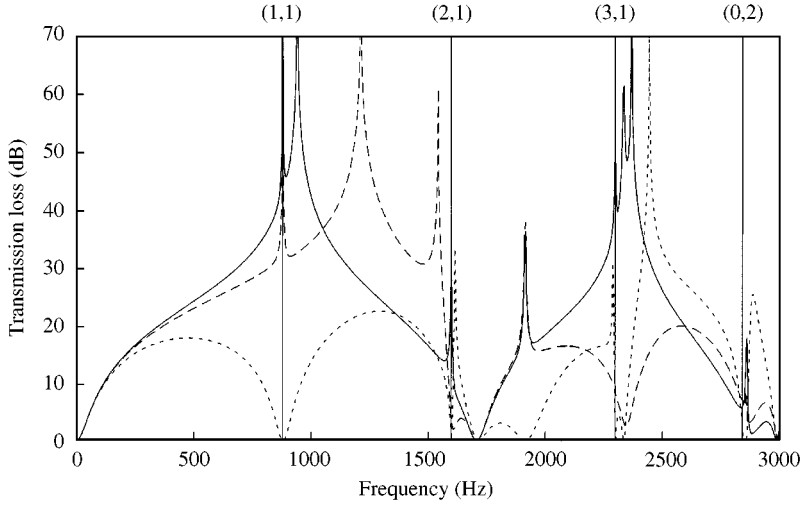

Figure 20. Analytical transmission loss of elliptical reversing chamber with $L = 0{\cdot}10$ m and eccentricity ε_1 ($a = 0{\cdot}23/2$ and $b = 0{\cdot}13/2$ m): ---, offset inlet and outlet with $\delta_1 = \delta_2 = 0{\cdot}06$ m; – – –, centred inlet, offset outlet with $\delta_2 = 0{\cdot}06$; ——, centred inlet, offset outlet with $\delta_2 = 0{\cdot}0479$ m.

the transmission loss even when the eccentricity is very low. In the case of expansion chambers, some slight deviations were found between the analytical and finite element results for a chamber length $L = 0{\cdot}05$ m. In the present case, these slight discrepancies appear for longer chambers with $L = 0{\cdot}10$ m.

Figures 19 and 20 show the benefits of using centred inlet and offset outlet, the latter located in the nodal line of the mode (2, 1), in long and short reversing chambers respectively. For comparison purposes, centred inlet and offset outlet with arbitrary offset outlet distance $\delta_2 = 0{\cdot}06$ m as well as offset inlet/outlet with $\delta_1 = \delta_2 = 0{\cdot}06$ m will be also analyzed. Considering a long chamber (see Figure 19), the case of offset inlet/outlet is found

to give the worst acoustic performance, since the mode (1, 1) starts to propagate at a frequency of 880 Hz. When the inlet is centred and the outlet is located at a suitable position, as it was defined previously (that is, $\delta_2 = x_c = 0{\cdot}0479$ m for the eccentricity ε_1), the mode (2, 1) cannot propagate and the cut-off frequency is moved up to 2840·88 Hz, associated with the mode (0, 2). In this situation, the acoustic attenuation of the reversing chamber is improved, increasing the frequency range of the repetitive peak behaviour of the plane wave model. The same geometries are considered in Figure 20, except the chamber length, which has been reduced to $L = 0{\cdot}10$ m. The effect of offsetting the inlet and outlet is quite relevant, since it changes the performance of the chamber drastically. In the case of offset inlet/outlet, the transmission loss exhibits the dome behaviour of an expansion chamber with wave propagation [9] along the major axis for frequencies below that associated with the mode (2, 1) and the first pass band appears at a frequency of 880 Hz (mode (1, 1)). By centring the inlet (dash line), the transmission loss is increased until the propagation of the mode (2, 1). Now the behaviour shows a resonant peak, and the domes do not appear. In addition, the benefits of the outlet location in the nodal line of this mode (solid line) can be observed but only in the high-frequency range.

7. CONCLUDING REMARKS

The acoustic attenuation performance of elliptical chamber mufflers has been studied, considering the effect of the chamber length, the relative inlet and outlet locations and the eccentricity of the cross-section. An analytical solution of the wave equation in elliptic co-ordinates, as well as finite elements and some experimental results have been used. The analytical solution is based on the modal decomposition of the acoustic field, and makes use of the point source method and Mathieu functions in order to account for the excitation of the modes. The mathematical complexity of the solution makes it difficult to find an analytical expression for the cut-off frequency of the different modes, as is available for the case of circular expansion chambers. Since the more critical issue related to the propagation of transversal modes is to obtain a proper definition of the applicability limit for the plane wave theory, it has been preferred to obtain a suitable polynomial fit for the cut-off frequency of the first propagating transversal mode, which is the even mode (2, 1) for concentric chambers and the even mode (1, 1) for non-concentric chambers with symmetry about the major axis. In addition, a polynomial fit has been obtained for a suitable location of the outlet when the propagation of the mode (2, 1) is intended to be suppressed. In the case of expansion chambers, the eccentricity has been found to play an important role in propagation of higher order modes, since the cut-off frequencies of these are reduced and the transmission loss collapses at a lower frequency in comparison to circular chambers with the same cross-section (the higher the eccentricity is, the lower the cut-off frequency will be). For ellipses with low eccentricity, the behaviour is found to be quite similar to that associated with the circular case. If reversing chambers are considered, the same comments can be applied regarding the reduction of the cut-off frequency, but now more differences appear between the circular geometry and the elliptic one with low eccentricity. Depending on the frequency range, the presence of evanescent modes and/or the propagation of elliptic higher order modes is more important since in this case the inlet and outlet ports are in close proximity.

ACKNOWLEDGMENT

The authors wish to thank the financial support received from CICYT to develop the project "Integración de Herrramientas Computacionales en el Desarrollo de Silenciadores

de Escape en Motores de Combustión Interna Alternativos", with reference TAP97-1270-C02.

REFERENCES

1. J. KIM and W. SOEDEL 1990 *Journal of Vibration and Acoustics* **112**, 452–459. Development of a general procedure to formulate four pole parameters by modal expansion and its application to three-dimensional cavities.
2. J.-G. IH and B.-H. LEE 1985 *Journal of the Acoustical Society of America* **77**, 1377–1388. Analysis of higher-order mode effects in the circular expansion chamber with mean flow.
3. J.-G. IH and B.-H. LEE 1987 *Journal of Sound and Vibration* **112**, 261–272. Theoretical prediction of the transmission loss of circular reversing chamber mufflers.
4. Y.-H. KIM and J. W. CHOI 1991 *Journal of Vibration and Acoustics* **113**, 543–550. General solution of acoustic wave equation for circular reversing chamber with temperature gradient.
5. M. ÅBOM 1990 *Journal of Sound and Vibration* **137**, 403–418. Derivation of four-pole parameters including higher order mode effects for expansion chamber mufflers with extended inlet and outlet.
6. A. SELAMET and P. M. RADAVICH 1997 *Journal of Sound and Vibration* **201**, 407–426. The effect of length on the acoustic attenuation performance of concentric expansion chambers: an analytical, computational and experimental investigation.
7. A. SELAMET and Z. L. JI 1998 *Journal of Sound and Vibration* **213**, 601–617. Acoustic attenuation performance of circular expansion chambers with offset inlet/outlet: I. Analytical approach.
8. A. SELAMET, Z. L. JI and P. M. RADAVICH 1998 *Journal of Sound and Vibration* **213**, 619–641. Acoustic attenuation performance of circular expansion chambers with offset inlet/outlet: II. Comparison with experimental and computational studies.
9. A. SELAMET and Z. L. JI 1998 *Journal of the Acoustical Society of America* **104**, 2867–2877. Acoustic attenuation performance of circular flow-reversing chambers.
10. A. SELAMET and Z. L. JI 1999 *Journal of Sound and Vibration* **223**, 197–212. Acoustic attenuation performance of circular expansion chambers with extended inlet/outlet.
11. B. K. WANG, K. Y. LAM, M. S. LEONG and P. S. KOOI 1994 *IEE Proceedings—Microwaves Antennas and Propagation* **141**, 483–488. Elliptical waveguide analysis using improved polynomial approximation.
12. S. CAORSI, M. PASTORINO and M. RAFETTO 1997 *IEEE Transactions on Antennas and Propagation* **45**, 926–935. Electromagnetic scattering by a multilayer elliptic cylinder under transverse-magnetic illumination: series solution in terms of Mathieu functions.
13. A. M. HUSSEIN and W. WURJARANTA 1997 *IEEE Transactions of Magnetics* **33**, 4125–4127. Analysis of elliptic conductors using the point matching method with Mathieu functions.
14. W. R. CALLAHAN 1964 *Journal of the Acoustical Society of America* **36**, 823–829. Flexural vibrations of elliptical plates when transverse shear and rotary inertia are considered.
15. K. SATO 1972 *Journal of the Acoustical Society of America* **52**, 919–922. Free flexural vibrations of an elliptical plate with simply supported edge.
16. K. HONG and J. KIM 1995 *Journal of Sound and Vibration* **183**, 327–351. Natural mode analysis of hollow and annular elliptical cylindrical cavities.
17. R. D. CISKOWSKI and C. A. BREBBIA 1991 *Boundary Element Methods in Acoustics*. Boston: Computational Mechanics Publications.
18. K. H. HUEBNER, E. A. THORNTON and T. G. BYROM 1995 *The Finite Element Method for Engineers*. New York: Wiley–Interscience; third edition.
19. M. ABRAMOWITZ and I. A. STEGUN 1972 *Handbook of Mathematical Functions*. New York: Dover Publications.
20. M. L. MUNJAL 1987 *Acoustics of Ducts and Mufflers*. New York: Wiley–Interscience.
21. F. PAYRI, J. M. DESANTES and A. BROATCH 2000 *Journal of the Acoustical Society of America* **107**, 731–738. Modified impulse method for the measurement of the frequency response of acoustic filters to weakly non linear transient excitations.